



Available online at www.sciencedirect.com



ScienceDirect

Trans. Nonferrous Met. Soc. China 25(2015) 483–489

Transactions of
Nonferrous Metals
Society of China

www.tnmsc.cn



Effect of cetyltrimethylammonium bromide on morphology and porous structure of mesoporous hydroxyapatite



Jing WANG¹, Su-ping HUANG¹, Kun HU¹, Ke-chao ZHOU¹, Hong SUN²

1. State Key Laboratory of Powder Metallurgy, Central South University, Changsha 410083, China;

2. Department of Otolaryngology Head and Neck Surgery, Xiangya Hospital,
Central South University, Changsha 410008, China

Received 10 February 2014; accepted 14 July 2014

Abstract: The mesoporous hydroxyapatite (HA) was synthesized by hydrothermal method utilizing cationic surfactant cetyltrimethylammonium bromide (CTAB) as template. The crystalline phase, morphology and porous structure were characterized respectively by different detecting techniques. The results reveal that the particles are highly crystalline hydroxyapatite phase. The surfactant has little influence on the morphology of the crystals, but affects the porous structure obviously. The sample without CTAB has a low surface area not exceeding $33\text{ m}^2/\text{g}$, and no distinct pores can be observed by TEM. While the samples obtained with the surfactant get better parameters. Numerous open-ended pores centered at 2–7 nm spread unequally on the surface of the hydroxyapatite nanorods. The N_2 adsorption–desorption experiments show type IV isotherms with distinct hysteresis loops, illustrating the presence of mesoporous structure. When the mole ratio of CTAB to HA is 1:2, the sample has the largest surface area of $97.1\text{ m}^2/\text{g}$ and pore volume of $0.466\text{ cm}^3/\text{g}$.

Key words: hydroxyapatite; cetyltrimethylammonium bromide; cationic surfactant; soft-template; mesoporous structure

1 Introduction

Since the MCM-41 silica molecular sieve was synthesized in 1992 [1], the inorganic mesoporous materials have attracted tremendous attention in the chemistry and material communities, due to their large surface area, narrow pore size distribution, regular 2D or 3D pore structures and thermal stabilities [2,3]. The outstanding properties make mesoporous materials potentially applicable in many fields of material science, ranging from chemical sensing unit [4] to drug delivery systems [5]. Recently, various mesoporous materials have been fabricated, including mesoporous metal oxides [6,7], aluminophosphates [8,9], metal (Zr, Ti, Sn, Ni and Fe) phosphate mesoporous molecular sieves [10], and the representative silica-based molecular sieves such as MCM, SBA, MSU and HMS[11]. Although these molecular sieves have tremendous applications in practice [12,13], they may not be suitable for tissue regeneration *in vivo* because of their indefinite biological

response [14].

Hydroxyapatite (HA), $\text{Ca}_{10}(\text{PO}_4)_6(\text{OH})_2$, is the major inorganic phase of human bones and teeth. It has been widely applied in biomedical engineering during the past decades as bone substitutes, such as bone cavity filler and bone cement, because of its excellent biocompatibility, bioactivity and suitable osteoconductivity [15,16]. Another relevant property of HA is the unique ability to adsorb a variety of chemical species on the surface. Many studies have employed HA with high performance liquid chromatography (HPLC) for separating proteins. Recently, mesoporous HA has attracted a great deal of attention as delivery systems for genes, proteins and drugs, due to the distinct advantages of highly ordered mesoporous structure, large surface area, and high loading capacity.

However, despite the favorable properties, the fabrication of meso-HA with large surface area is difficult owing to its preferable crystallization in aqueous solution and then cannot interact with surfactant molecules. Most of mesoporous hydroxyapatite has the

Foundation item: Projects (51102285, 81170912) supported by the National Natural Science Foundation of China; Project supported by the Open Foundation of State Key Laboratory of Powder Metallurgy, China

Corresponding author: Su-ping HUANG; Tel: +86-13975803269; E-mail: huangsp1@csu.edu.cn
DOI: 10.1016/S1003-6326(15)63628-7

surface area of 20–60 m²/g. Therefore, a number of studies have been focused on the synthesis of hydroxyapatite with organized mesoporosity and controllable morphologies, such as sol–gel method, hydrothermal method, precipitation method, mechanochemical treatment, microemulsion process and templating techniques [17,18]. YOSHIMURA et al [19] prepared the needle-like HA whiskers with a length of 10–30 μm and diameter of 0.1–1 μm with hydrothermal method. BEZZI et al [20] synthesized pure HA powders with macropores (20 μm in size) by a novel and simple sol–gel method. Among these techniques, surfactant templating method is considered to be an effective way to control the morphology and porosity of HA particles. During the formation of meso-HA the surfactants could assemble together with inorganic phases, forming an inorganic–organic network as nucleation center, and subsequently produce regular pore structure when they are removed [15]. A series of surfactants, including pluronic P123 [21], sodium dodecyl sulfate (SDS) [22], and cetyltrimethylammonium bromide (CTAB) [16,23], have been utilized as templates to synthesize meso-HA particles. For example, LI et al [16] synthesized HA utilizing CTAB and studied the impact of reaction temperature and CTAB/PO₄³⁻ ratio on the phase, morphology and thermal stability. COELHO et al [23] synthesized HA nanorods with CTAB and discussed the effect of the sintering temperature on the morphological and crystallographic characteristics.

In this work, the meso-HA particles were synthesized via hydrothermal method utilizing CTAB as template, and the effects of mole ratio of CTAB to HA on the morphology, surface area and porous structure of the particles were discussed.

2 Experimental

2.1 Materials

Cetyltrimethylammonium bromide (CTAB) was purchased from Tianjin Guangfu Fine Chemical Industry Research Institute, China. (NH₄)₂HPO₄ was purchased from Tianjin Bodi Chemical Co., Ltd., China. Ca(NO₃)₂·4H₂O was purchased from Tianjin Hengxing Chemical Co., Ltd., China. And ammonium hydroxide (NH₃·H₂O) was purchased from Zhuzhou Quartzification Glass Co., Ltd., China. All reagents were analytical grades and used directly without further purification.

2.2 Synthesis

(NH₄)₂HPO₄ and Ca(NO₃)₂·4H₂O were used as phosphorus and calcium sources, and the cationic surfactant CTAB was utilized as the template in the synthesis of meso-HA particles. Five gradient experiments were carried out with different amount of

CTAB (the mole ratios of CTAB to HA were 1:2, 1:1, 5:4, 3:2 and 2:1, respectively). Firstly, appropriate amount of CTAB was dissolved in 50 mL deionized water, and 0.98 g (NH₄)₂HPO₄ was then added into the solution (designated as solution 1). The pH value of solution 1 was adjusted to 10 with NH₃·H₂O. And 2.96 g Ca(NO₃)₂·4H₂O was dissolved in 50 mL deionized water (designated as solution 2). Subsequently, solution 2 was added dropwise into solution 1 with continuous and vigorous magnetic stirring, while the pH value of the mixed solution was maintained higher than 10 by adding NH₃·H₂O. The prepared suspension was then transferred to Teflon autoclaves and crystallized at 120 °C for 3 h. After being centrifuged, the obtained precipitate was washed three times with deionized water, and soaked in anhydrous ethanol at 60 °C for 72 h to remove the template. Finally, the samples synthesized with different amount of CTAB were dried in an oven at 100 °C for 24 h, and designated as H₁, H₂, H₃, H₄ and H₅, respectively. The sample synthesized without CTAB (designated as H₀) was used for comparison.

2.3 Characterization

Wide angle X-ray diffraction (XRD) patterns of the samples were measured on a Rigaku D/max-2550 diffractometer with Cu K_α radiation (1.5419 Å). The diffractometer was operated at a voltage of 40 kV and a current of 250 mA, and the data were collected by scanning the powder in 2θ range of 10°–70° with incremental step of 0.02°. Fourier transform infrared spectroscopy (FT-IR) was used to investigate the chemical and structural compositions of the samples with KBr pellet. The spectra were recorded from 4000 cm⁻¹ to 400 cm⁻¹ on a Nicolet 6700 spectrophotometer. The morphology and the porous structure of HA particles were observed via a JEM-2100F transmission electron microscopy (TEM) operating at 200 kV. Nitrogen adsorption–desorption isotherms were obtained on a Quantachrome Autosorb automatic analyzer at liquid nitrogen temperature. All the samples were degassed at 473 K for 24 h before the measurement. The surface areas were calculated from Barrett–Emmett–Teller (BET) equation at the relative pressure ranging from 0.15 to 0.3, and the pore parameters were calculated based on Barrett–Joyner–Halanda (BJH) model from the desorption branches of the isotherms.

3 Results and discussion

3.1 XRD characterization of HA samples

The XRD patterns of the samples with different amount of CTAB are shown in Fig. 1. The diffraction peaks and the lattice parameters of the six samples correspond well to the standard data of hexagonal

hydroxyapatite on JCPDS card No. 24–0033. No other secondary phase is observed in the patterns, implying that all the samples are phase-pure hydroxyapatite crystals with the space group of $P6_3/m$. The sharp peaks demonstrate the high crystallization of the particles. There is no significant difference in XRD patterns between blank HA and those synthesized with CTAB, indicating that the surfactant cannot induce the crystallization of any secondary phases and has little influence on the crystallization of HA particles. The average crystallite sizes and the lattice parameters are presented in Table 1. The crystallite sizes are calculated from Scherrer equation using (002) diffraction peak: $d=k\lambda/(\beta_{1/2}\cos\theta)$, where the constant k is 0.9, the wavelength λ is 1.5418 Å, the diffraction angle 2θ is 25.82° for the reflection (002), and diffraction peak width $\beta_{1/2}$, expressed in radian, is equal to half of the peak height.

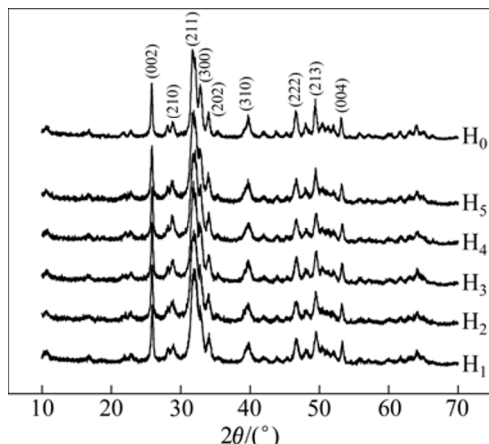


Fig. 1 XRD patterns of HA particles: H_0 —Without CTAB; H_1 — $n(\text{CTAB}):n(\text{HA})=1:2$; H_2 — $n(\text{CTAB}):n(\text{HA})=1:1$; H_3 — $n(\text{CTAB}):n(\text{HA})=5:4$; H_4 — $n(\text{CTAB}):n(\text{HA})=3:2$; H_5 — $n(\text{CTAB}):n(\text{HA})=2:1$

3.2 FTIR characterization of HA samples

The FT-IR spectra of CTAB and HA particles synthesized with different amount of CTAB are presented in Fig. 2. The spectra of the six samples are

similar to each other, showing all the stretching and bending vibrations of the PO_4^{3-} and OH^- functional groups. The bands at 3571 and 631 cm⁻¹ are stretching vibrations of hydroxyl functional groups. The absorption peaks at 566 and 604 cm⁻¹ indicate the presence of v_4 phosphate bending mode. The peaks at 964, 1035 and 474 cm⁻¹ are attributed to v_1 , v_3 phosphate stretching modes and v_2 phosphate bending mode, respectively. The characteristic peaks of NH_4^+ ($\nu(\text{NH}_4^+)$ at 3170 cm⁻¹ and $\delta(\text{NH}_4^+)$ at 1384 cm⁻¹) are observed in the spectra, implying the existence of ammonium salt. The broad bands at around 3426 and 1634 cm⁻¹ confirm the presence of adsorbed water in the samples. The characteristic peaks of CTAB ($\nu^{\text{as}}(\text{C—H})$ at 2927 cm⁻¹ and $\nu^{\text{a}}(\text{C—H})$ at 2852 cm⁻¹) could be found in the spectra of samples H_1 – H_5 . The appearance of these two

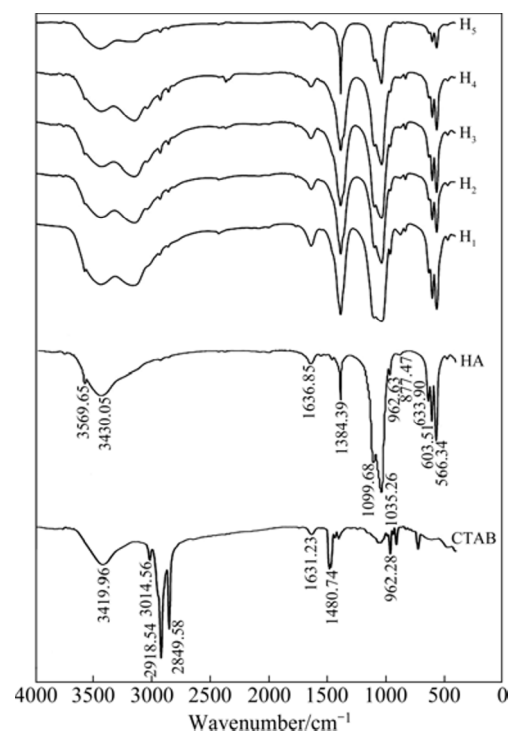


Fig. 2 FT-IR spectra of CTAB and HA particles synthesized with different amount of CTAB

Table 1 Parameters of samples synthesized with different amount of CTAB

Sample	$n(\text{CTAB}):n(\text{HA})$	$S_{\text{BET}}^{(1)}$ /(m ² ·g ⁻¹)	Average pore size ⁽²⁾ /nm	Pore volume ⁽²⁾ /(cm ³ ·g ⁻¹)	Lattice constant/Å		Crystallite size ⁽³⁾ /nm
					a	c	
H_0	0	32.462	29.095	0.368	9.438	6.883	21.5
H_1	1:2	97.115	58.455	0.466	9.427	6.874	20.5
H_2	1:1	79.484	16.450	0.419	9.452	6.865	20.3
H_3	5:4	80.244	29.053	0.444	9.417	6.864	31.8
H_4	3:2	82.085	82.135	0.427	9.434	6.862	21.3
H_5	2:1	74.888	16.525	0.399	9.422	6.874	36.1

1) Calculated from Barrett–Emmett–Teller equation; 2) Calculated based on Barrett–Joyner–Halanda model; 3) Calculated by Debye–Scherrer equation

peaks indicates that the template has not been removed completely by soaking the precipitate in anhydrous ethanol. The weak peaks at around 875 cm^{-1} in samples H_1-H_4 are the CO_3^{2-} carbonate mode of vibration, revealing that a certain level of carbonate substitution might have taken place in the synthesis process. The carbonate ions may be originated from a reaction between atmospheric carbon dioxide and the solution during the synthesis process, or from the organic templates [24].

3.3 Morphology of HA samples

The morphology and porous structure of HA particles are clearly demonstrated by transmission electron microscopy (TEM). As shown in Fig. 3, similar rod-like particles with an average diameter of 10–20 nm and a length of 60–100 nm are obtained in the six

samples, including the one synthesized without the surfactant. Despite the little influence on the morphology, the presence of CTAB obviously affects the porous structure of HA particles. For sample H_0 , no mesoporous structure could be observed; while for samples H_1-H_5 , numerous disconnected pores with a size of 2–7 nm (white dots in relevant images) spread unequally around the surface of the nanorods. The selected area electron diffraction (SAED) pattern and the high resolution TEM (HRTEM) image of H_1 are also shown in Fig. 3.

The formation of the rod-like hydroxyapatite mesoporous particles may result from the crystallization of these particles on the surface of the long rod-like surfactant micelles. As a cationic surfactant, CTAB consists of two parts: a positively charged hydrophilic head with strong affinity for water molecules and a hydrophobic tail with less affinity for water molecules.

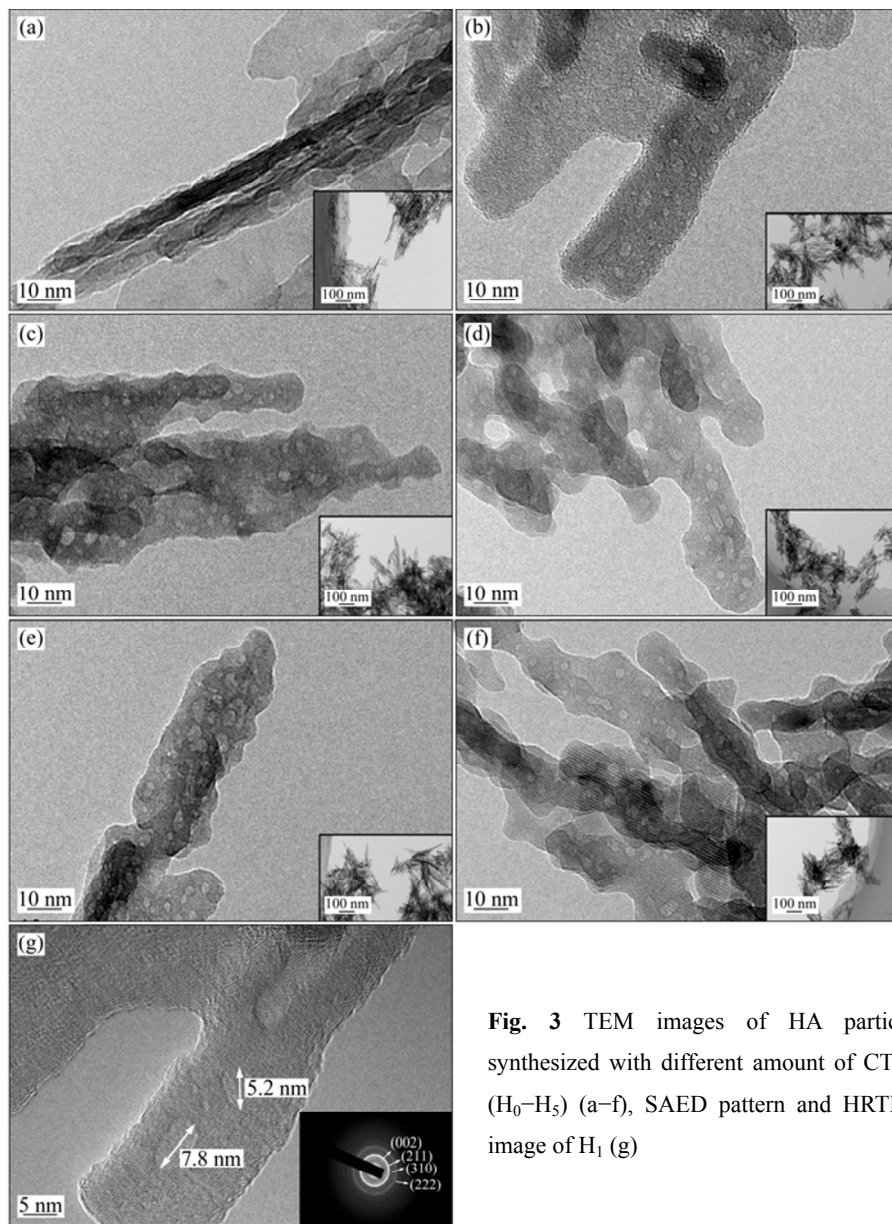


Fig. 3 TEM images of HA particles synthesized with different amount of CTAB (H_0-H_5) (a–f), SAED pattern and HRTEM image of H_1 (g)

The surfactant generates monomers in aqueous solution. When the surfactant concentration increases, the monomers form micelles by self-assembly with their hydrocarbon chains inside. Then the surface of micelles is positively charged. After adding PO_4^{3-} into the surfactant solution, these anions would be attracted to the micelles surface due to the electrostatic attraction between them. In addition, both CTA^+ and PO_4^{3-} have the same tetrahedral structure, which could make them stereochemically compatible to interact with each other in an effective manner [25]. Therefore, hexagonal $\text{CTA}^+-\text{PO}_4^{3-}$ complex micelles in the solution are formed possibly due to electrostatic attraction and complementary stereochemistry between the micelles and phosphate anions. The hexagonal complex micelles might act as a nucleation center for the formation of hydroxyapatite. When Ca^{2+} is added into the solution, it combines immediately with the surface of $\text{CTA}^+-\text{PO}_4^{3-}$ complex micelles, by the electrostatic attraction of PO_4^{3-} .

Then, the reaction takes place on the hydrophilic surface of the micelles, and the rod-like structure of HA–CTAB complex is formed. Subsequently, the mesoporous will be generated after the removal of the surfactant [16,25].

3.4 Porosity analysis of HA samples

Figure 4 shows the respective N_2 adsorption–desorption isotherms of HA particles synthesized with different amount of CTAB. The isotherms of samples H_1 – H_5 can be categorized as type IV curves with distinct hysteresis loops. Type IV isotherms illustrate the presence of mesoporous structure, which convincingly corroborates the TEM results. The irreversibility between adsorption and desorption processes leads to the appearance of hysteresis loops in these isotherms. The type H_3 loops are attributed to the large slit-shaped pores caused by the aggregation of particles. And due to the presence of these large pores, the capillary condensations occur at high relative

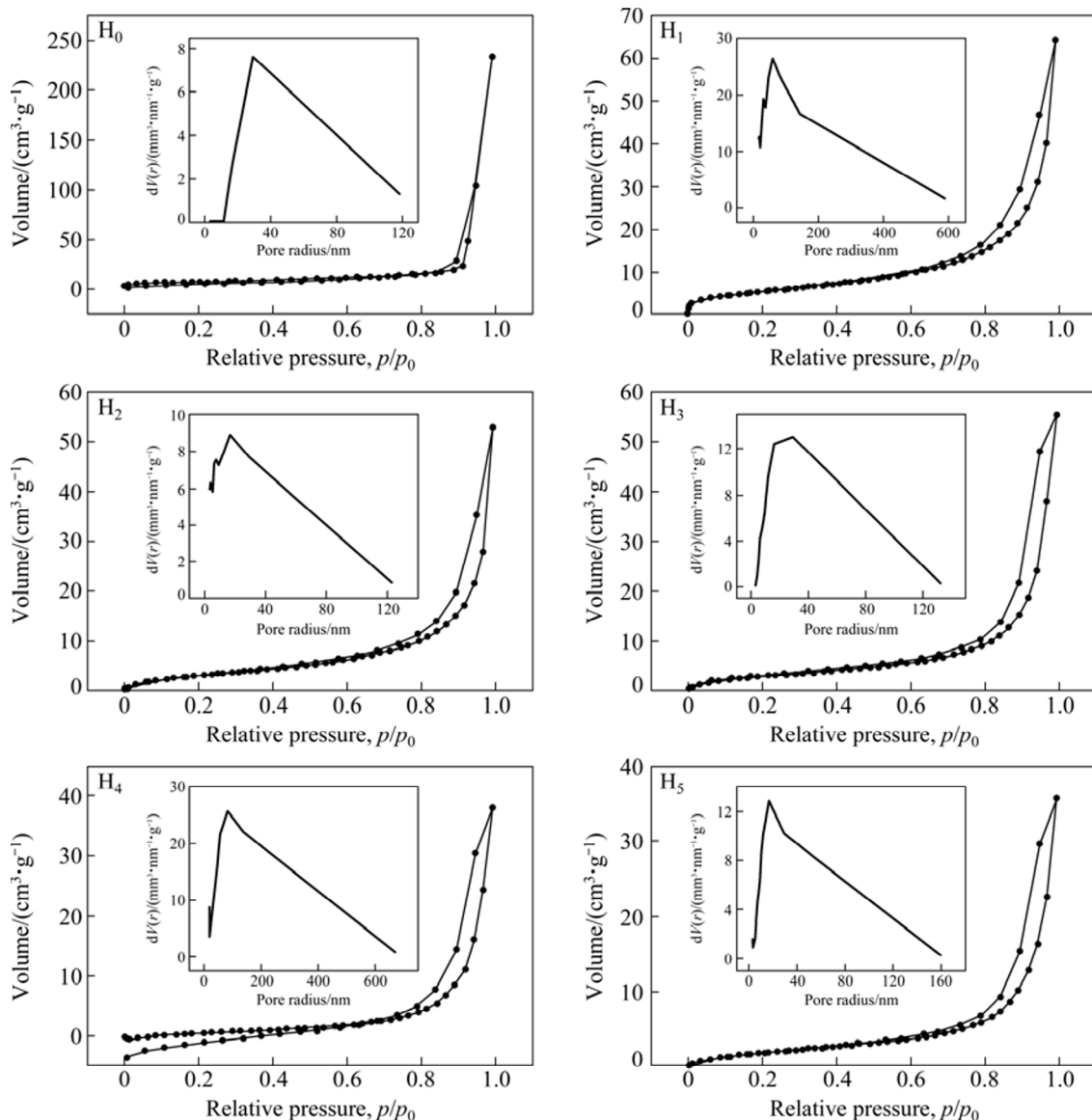


Fig. 4 N_2 adsorption–desorption isotherms and pore size distribution graphs

pressures (p/p_0) and adsorption saturations are not visible. The separation at the starting point of H_4 isotherms mainly results from the lack of the sample during the test. The parameters of the samples calculated from the desorption branch of the isotherms are shown in Table 1. The sample with the least amount of surfactant has the largest pore volume of $0.466 \text{ cm}^3/\text{g}$ and the largest surface area of $97.115 \text{ m}^2/\text{g}$. Without the presence of CTAB, the sample gets a small surface area of $33 \text{ m}^2/\text{g}$. The pore volume of the samples mainly decreases with the increase of surfactant amount, except for one case in which the mole ratio of CTAB to HA is 1:1. The pore size distribution is calculated based on Barrett–Joyner–Halanda (BJH) model. Each sample exhibits a broad distribution curve with a distinct peak, while samples H_1 and H_2 are accompanied with another small peak. The calculated pore sizes of the samples deviate far from the average values obtained from TEM images, especially for sample H_1 with the pore size centered approximately at 58 nm, and sample H_4 at 82 nm. It may be attributed to the agglomeration of the nanorods. And the calculated pore sizes mainly reveal the voids of the agglomerated particles.

4 Conclusions

1) The HA particles with mesoporous structure were synthesized by hydrothermal method utilizing CTAB as template. The surfactant does not induce the crystallization of any secondary phase and has little influence on the crystallization of HA particles.

2) The presence of cationic surfactant CTAB has an evident effect on the mesoporous structure of HA particles, including the surface area, the pore volume and the pore size. The sample without CTAB has a small surface area not exceeding $33 \text{ m}^2/\text{g}$, and no distinct pores could be observed. The samples obtained with the existence of the surfactant have better parameters. Numerous open-ended pores of 2–7 nm could be easily found through the nanorods.

3) The particles with the least amount of CTAB have the largest pore volume of $0.466 \text{ cm}^3/\text{g}$ and surface area of $97.115 \text{ m}^2/\text{g}$.

References

- [1] KRESGE C T, LEONOWICA M E, ROTHW W J, VARTULI J C, BECK J S. Ordered mesoporous molecular sieves synthesized by a liquid-crystal template mechanism [J]. *Nature*, 1992, 359(6397): 710–712.
- [2] YANG Pei-dong, ZHAO Dong-yuan, MARGOLESE D I, CHMELKA B F, STUCKY G D. Generalized syntheses of large-pore mesoporous metal oxides with semicrystalline frameworks [J]. *Nature*, 1998, 396(6707): 152–155.
- [3] YANG Pei-dong, ZHAO Dong-yuan, MARGOLESE D I, CHMELKA B F, STUCKY G D. Block copolymer templating syntheses of mesoporous metal oxides with large ordering lengths and semicrystalline framework [J]. *Chemistry of Materials*, 1999, 11(10): 2813–2826.
- [4] TORRENT-BURGUES J, RODRIGUEZ-CLEMENTE R. Hydroxyapatite precipitation in a semibatch process [J]. *Crystal Research and Technology*, 2001, 36(8–10): 1075–1082.
- [5] FAGUNDES L B, SOUSA T G F, SOUSA A, SILVA V V, SOUSA E M B. SBA-15-collagen hybrid material for drug delivery applications [J]. *Journal of Non-crystalline Solids*, 2006, 352(32–35): 3496–3501.
- [6] HUDSON M J, KNOWLES J A. Preparation and characterisation of mesoporous, high-surface-area zirconium (IV) oxide [J]. *Journal of Material Chemistry*, 1996, 6(1): 89–95.
- [7] BEHRENS P. Voids in variable chemical surroundings: Mesoporous metal oxides [J]. *Angewandte Chemie (International Edition in English)*, 1996, 35(5): 515–518.
- [8] KIMURA T, SUGAHARA Y, KURODA K. Synthesis of mesoporous aluminophosphates and their adsorption properties [J]. *Microporous and Mesoporous Materials*, 1998, 22(1–3): 115–126.
- [9] PETRAKIS D E, HUDSON M J, POMONIS P J, SDOUKOS A T, BAKAS T V. Synthesis and properties of some mesoporous aluminophosphates with acidic surface sites [J]. *Journal of Material Chemistry*, 1995, 5(11): 1975–1983.
- [10] THIEME M, SCHUTH F. Preparation of a mesoporous high surface area titanium oxo phosphate via a non-ionic surfactant route [J]. *Microporous and Mesoporous Materials*, 1999, 27(2–3): 193–200.
- [11] TANEV P T, PINNAVAIA T J. A neutral templating route to mesoporous molecular sieves [J]. *Science*, 1995, 267(5199): 865–867.
- [12] DAI Cheng-long, GUO Han, LU Jing-xiong, SHI Jian-lin, WEI Jie, LIU Chang-sheng. Osteogenic evaluation of calcium/magnesium-doped mesoporous silica scaffold with incorporation of rhBMP-2 by synchrotron radiation-based μ CT [J]. *Biomaterials*, 2011, 32(33): 8506–8517.
- [13] DAI Cheng-long, YUAN Yuan, LIU Chang-sheng, WEI Jie, HONG Hua, LI Xiao-sheng, PAN Xiao-hua. Degradable, antibacterial silver exchanged mesoporous silica spheres for hemorrhage control [J]. *Biomaterials*, 2009, 30(29): 5364–5375.
- [14] ZENG Fan-yan, WANG Jing, WU Yi, YU Yuan-man, TANG Wei, YIN Man-li, LIU Chang-sheng. Preparation of pore expanded mesoporous hydroxyapatite via auxiliary solubilizing template method [J]. *Colloids and Surfaces A: Physico-chemical and Engineering Aspects*, 2014, 441: 737–743.
- [15] SHANTHI P M S L, MANGALARAGA R V, UTHIRAKUMAR A P, VELMATHI S, ASHOK M, BALASUBRAMANIAN T. Synthesis and characterization of porous shell-like nano hydroxyapatite using cetyltrimide as template [J]. *Journal of Colloid and Interface Science*, 2010, 350(1): 39–43.
- [16] LI Y B, TJANDRA W, TAM K C. Synthesis and characterization of nanoporous hydroxyapatite using cationic surfactants as templates [J]. *Materials Research Bulletin*, 2008, 43(8–9): 2318–2326.
- [17] BIGI A, BOANINI E, RUBINI K. Hydroxyapatite gels and nanocrystals prepared through a sol–gel process [J]. *Journal of Solid State Chemistry*, 2004, 177(9): 3092–3098.
- [18] MOBASHERPOUR I, SOULATI HESHAJIN M, KAZEMZADEH A, ZAKERI M. Synthesis of nanocrystalline hydroxyapatite by using precipitation method [J]. *Journal of Alloys and Compounds*, 2007, 430(1–2): 330–333.
- [19] YOSHIMURA M, SUDA H, OKAMOTO K, IOKU K. Hydrothermal synthesis of biocompatible whiskers [J]. *Journal of Materials Science*, 1994, 29(13): 3399–3402.

- [20] BEZZI G, CELOTTI G, LANDI E, LA TORRETTA T M G, SOPYAN I, TAMPIERI A. A novel sol-gel technique for hydroxyapatite preparation [J]. Materials Chemistry and Physics, 2003, 78(3): 816–824.
- [21] NG S X, GUO J, MA J, LOO S C J. Synthesis of high surface area mesostructured calcium phosphate particles [J]. Acta Biomaterialia, 2010, 6(9): 3772–3781.
- [22] ZHANG Jing-xian, FUJIWARA M, XU Qiang, ZHU Ying-chun, IWASA M, JIANG Dong-liang. Synthesis of mesoporous calcium phosphate using hybrid templates [J]. Microporous and Mesoporous Materials, 2008, 111(1): 411–416.
- [23] COELHO J M, MOREIRA J A, ALMEIDA A, MONTEIRO F J. Synthesis and characterization of HA_p nanorods from a cationic surfactant template method [J]. Journal of Materials Science, 2010, 21(9): 2543–2549.
- [24] WU Xiao-dong, SONG Xiao-feng, LI Dong-song, LIU Jian-guo, ZHANG Pei-biao, CHEN Xue-si. Preparation of mesoporous nano-hydroxyapatite using a surfactant template method for protein delivery [J]. Journal of Bionic Engineering, 2012, 9(2): 224–233.
- [25] VERMA G, BARICK K C, MANOJ N, SAHU A K, HASSAN P A. Rod-like micelle templated synthesis of porous hydroxyapatite [J]. Ceramics International, 2013, 39(8): 8995–9002.

CTAB 对于介孔羟基磷灰石形貌和孔结构的影响

王 晶¹, 黄苏萍¹, 胡 塟¹, 周科朝¹, 孙 虹²

1. 中南大学 粉末冶金国家重点实验室, 长沙 410083;

2. 中南大学 湘雅医院 耳鼻喉头颈外科, 长沙 410008

摘要: 以阳离子表面活性剂十六烷基三甲基溴化铵(CTAB)为模板剂, 采用水热法合成介孔羟基磷灰石, 并利用不同检测手段对其物相、形貌和孔结构进行表征。结果表明, 合成物是高度结晶的羟基磷灰石相。表面活性剂对催化剂晶粒的形貌影响较小, 但明显影响孔结构的形成。无表面活性剂存在时晶粒的比表面积较小($\leq 33 \text{ m}^2/\text{g}$), 通过 TEM 无法观察到明显的孔结构。而对于有表面活性剂存在时合成的样品, 可以看到许多孔径大小为 2~7 nm 的开孔, 不均匀地分布在羟基磷灰石纳米棒的表面。氮气吸附-脱附实验得到的均为吸附 IV 型等温线, 并伴有明显的滞后环, 证实了介孔结构的存在。当 CTAB 与羟基磷灰石的摩尔比为 1:2 时, 样品的比表面积与孔容最大, 其比表面积为 $97.1 \text{ m}^2/\text{g}$, 孔容为 $0.466 \text{ cm}^3/\text{g}$ 。

关键词: 羟基磷灰石; 十六烷基三甲基溴化铵; 阳离子表面活性剂; 软模板法; 介孔结构

(Edited by Wei-ping CHEN)